

Optimal sliding mode controller for lower limb rehabilitation exoskeleton in constrained environments

Mohammad A. Faraj^{1,2}, Boutheina Maalej¹, Nabil Derbel¹

¹Laboratory of Control and Energy Management, Ecole Nationale D'ingénieurs De Sfax, University of Sfax, Sfax, Tunisia

²Department of Electrical Engineering, College of Engineering, University of Anbar, Ramadi, Iraq

Article Info

Article history:

Received Jan 1, 2023

Revised Jan 29, 2023

Accepted Feb 4, 2023

Keywords:

Grey wolf optimization algorithm

Holonomic constrained

Lower limb exoskeleton

Rehabilitation robots

Sliding mode control

ABSTRACT

In this article, a lower limb exoskeleton (LLE) under contacting constrained motion has been modelled using augmented Lagrange equations which include Lagrange multiplier and Jacobian vectors. A sliding mode Controller optimized by the grey Wolf optimization algorithm has been used for controlling (LLE) in the case of constrained motion with uncertainties and outside perturbation. The grey wolf optimization algorithm has been used as an optimization algorithm for finding the optimal controllers' parameters in order to improve the performance of the system. The stability analysis of the closed-loop system has been performed using Lyapunov theory of stability. To validate the effectiveness of the proposed controller structure grey wolf optimization algorithm controller (GW-SMC), a series of comparative simulations have been carried out with other types of recently existing sliding mode control (SMC). The results of numerical simulations indicate the superiority of the sliding mode optimized by the GW-SMC over other types of recently existing controller in terms of tracking errors and robustness towards uncertainties and external disturbances.

This is an open access article under the [CC BY-SA](https://creativecommons.org/licenses/by-sa/4.0/) license.



Corresponding Author:

Mohammad A. Faraj

Department of Electrical Engineering, College of Engineering, University of Anbar

Ramadi, Iraq

Email: Mohammed.faraj@uoanbar.edu.iq

1. INTRODUCTION

In the last decades, stroke illness has been considered as one of the most well-known diseases for humans in the all sides of the world. Stroke illness has been considered as the main cause of human nervous system damage, lower limb function disorders and hemiplegia [1]. As a result, the rehabilitation process of stroke patients has become an urgent thing to be undertaken to solve the disorder motion of aging humans that suffer from the stroke case [2]. Traditionally, the classical physical therapy is performed by rehabilitation therapists in manual manner. However, this manual process become tedious and exhausted strategy to the physical therapists while they try to help the stroke patients in process of recovering the gait of them. As a an effective and sufficient kinds of the rehabilitation robots, lower limb rehabilitation exoskeletons (LLE) have been used as an effective rehabilitation approach for stroke patients with motion disorder [3]. Various types of LLE have been manufactured and constructed by different universities and research centers such as Lokomat [4], berkeley lower extremity exoskeleton (BLEEX) [5] and active leg exoskeleton (ALEX) [6]. Different control strategies have been introduced in order to track predetermined trajectory for nonlinear robotics systems such as: active disturbance rejection control [7], fractional order control [8], robust control [9] and sliding mode control (SMC) [10].

In fact, SMC has been adopted as an effective and adequate controller for trajectory tracking of linear and highly coupled non-linear robotic rehabilitation systems because of having the distinguished properties of

SMC represented by the insensitivity against the variations in parameters and the external perturbations [11], [12]. These unique attributes enable the SMC to be used for different applications with various combination such as: impedance control for rehabilitation exoskeletons [13], and hybrid adaptive robust control for lower limb exoskeleton [14]. The sliding mode control is also used as an efficient controller for delta parallel robot [15] and for wind turbines [16]. The tuning parameters of SMC controllers represent an important issue on the system performance. The incorrect tuning of the parameters may lead to decreasing the controller performance [17]. So, to get an excellent performance, a meta-heuristic optimization technique adopted from natural behavior of animals has been used in last decades. In the present study, grey wolf optimization (GWO) has been used to optimize the tuning factors of developed sliding mode controller. Traditionally, the dynamic equations of lower limb robotic exoskeletons have been developed using popular Lagrange equations [18]. In fact, the contacting of robotic systems with horizontal or vertical surface modified the Lagrange equations to include the Lagrange multiplier and Jacobian vectors in its formula [19], [20]. Most of previous works in literature have modeled LLE without taking in to consideration the contacting of LLE with the ground (constraint motion). Hence, the primary objective of this article is to model and control the LLE in case of contacting with ground. To the best of author's knowledge, the modeling and controlling of LLE in constraint motions have not been discussed deeply in literature. The rest of this paper is constructed as follows: The derivation of dynamic equations of the LLE in constraint motions is accomplished in the section 2. The optimal sliding mode control law are developed in section 3. In the section 4, the results of the work have been explained and discussed. The conclusion of this article is achieved in the section 5.

2. METHOD

2.1. Modeling of lower limb exoskeleton in free motion

The dynamic model of the LLE with three degrees of freedom has been adopted in this study as indicated in Figure 1. Figure 1(a) represents the free motion of LLE, whereas Figure 1(b) stands for constrained motion of LLE. In free motion, classical Lagrange equations are used to model the dynamic equation of LLE as shown Figure 1(a) where O is the coordinate origin and *h* refers to the distance from the coordinate origin O at hip joint to the point of contacting of LLE with the ground and $\phi(q)$ refers to an algebraic constraint equation that represent the constraint motion in joint space [21], [22]. The Euler-Lagrange formulas are normally used to derive the dynamic model equations of the lower limb exoskeleton, which can be expressed as:

$$M(q)\ddot{q} + C(q, \dot{q})\dot{q} + G(q) + \tau_d = \tau \tag{1}$$

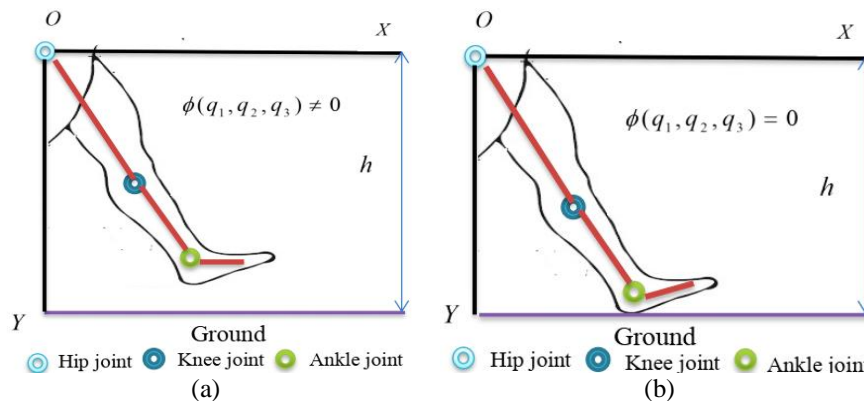


Figure 1. Three-link exoskeleton structure in (a) free motion and (b) constraint motion

where: $q, \dot{q}, \ddot{q} \in \mathbb{R}^3$ are angular joint position, velocity and acceleration vectors respectively. $M(q) \in \mathbb{R}^{3 \times 3}$ stands for positive definite inertia matrix. $C(q, \dot{q})\dot{q} \in \mathbb{R}^3$ represents Coriolis, centrifugal forces and torques. $G(q) \in \mathbb{R}^3$ are the torques of the gravity and $\tau \in \mathbb{R}^3$ is the vector of joint torques and $\tau_d \in \mathbb{R}^3$ is the bounded unknown external disturbances at LLE joints. The contents of $M(q)$, $C(q, \dot{q})\dot{q}$ and $G(q)$ of three joints of LLE are:

$$M_{11} = a_1 + a_2 + a_4 + 2 a_3 \cos(q_2) + 2a_5 \cos(q_2 + q_3) + 2a_6 \cos(q_3)$$

$$M_{12} = M_{21} = a_2 + a_4 + a_3 \cos(q_2) + a_5 \cos(q_2 + q_3) + 2a_6 \cos(q_3)$$

$$\begin{aligned}
M_{13} &= M_{31} = a_4 + a_5 \cos(q_2 + q_3) + 2a_6 \cos(q_3), M_{22} = a_2 + a_4 + 2a_6 \cos(q_3) \\
M_{23} &= M_{23}a_4 + 2a_6 \cos(q_3), M_{33} = a_4 \\
C_{11} &= -a_5(\dot{q}_2 + \dot{q}_3) \sin(q_2 + q_3) - a_3\dot{q}_2 \sin(q_2) - a_6\dot{q}_3 \sin(q_3) \\
C_{12} &= -a_5(\dot{q}_1 + \dot{q}_2 + \dot{q}_3) \sin(q_2 + q_3) - a_3(\dot{q}_1 + \dot{q}_2) \sin(q_2) - a_6\dot{q}_3 \sin(q_3) \\
C_{13} &= -a_5(\dot{q}_1 + \dot{q}_2 + \dot{q}_3) \sin(q_2 + q_3) - a_3 \sin(q_2) - a_6(\dot{q}_1 + \dot{q}_2 + \dot{q}_3) \sin(q_3) \\
C_{21} &= -a_5\dot{q}_1 \sin(q_2 + q_3) + a_3\dot{q}_1 \sin(q_2) - a_6\dot{q}_3 \sin(q_3), C_{22} = -a_6\dot{q}_3 \sin(q_3) \\
C_{23} &= -a_6(\dot{q}_1 + \dot{q}_2 + \dot{q}_3) \sin(q_3) \\
C_{31} &= a_5\dot{q}_1 \sin(q_2 + q_3) + a_6(\dot{q}_1 + \dot{q}_2) \sin(q_3), C_{32} = a_6(\dot{q}_1 + \dot{q}_2) \sin(q_3), C_{33} = 0 \\
G_1 &= -[b_1 \sin(q_1) + b_2 \sin(q_1 + q_2) + b_3 \sin(q_1 + q_2 + q_3)] \\
G_2 &= -[b_2 \sin(q_1 + q_2) + b_3 \sin(q_1 + q_2 + q_3)], G_3 = -[b_3 \sin(q_1 + q_2 + q_3)] \\
b_1 &= (m_1 d_1 + m_2 l_1 + m_3 l_1)g, b_2 = (m_2 d_2 + m_3 l_2)g, b_3 = m_3 d_3 g \\
a_1 &= I_1 + m_1 d_1^2 + (m_2 + m_3)l_1^2, a_2 = I_2 + m_2 d_2^2 + m_3 l_2^2, a_3 = (m_2 d_2 + m_3 l_2)l_1 \\
a_4 &= I_3 + m_3 d_3^2, a_5 = m_3 d_3 l_1, a_6 = m_3 d_3 l_2
\end{aligned}
\tag{2}$$

where: $m_1, m_2, m_3, l_1, l_2, l_3$, refer to masses and lengths of thigh, shank, and foot links of the human lower limb and exoskeleton respectively. d_1, d_2, d_3 stand for the position of the center of mass of thigh, shank and foot of LLE and human lower limb respectively. I_1, I_2, I_3 stands for the moments of inertia of thigh, shank and foot of the exoskeleton and human lower limb respectively and g is the gravity acceleration.

2.2. Modeling of lower limb exoskeleton in constrained motion

During constrained motion, the LLE is in contact with ground and can be viewed as a closed loop chain. Thus, as shown in (1) of free motion can not be applied when we want to describe the dynamic equations of the LLE when contacting with the ground as shown in Figure 1(b). In this case, a holonomic constraint illustrated by an algebraic equation in joint space is used to describe the contacting of LLE with ground [22], [23].

$$\phi(q) = l_1 \cos(q_1) + l_2 \cos(q_1 + q_2) + l_3 \cos(q_1 + q_2 + q_3) - h \tag{3}$$

Owing to these constraint circumstances, the term $\tau = J(q)^T \lambda$ must be added to dynamic in (1). The Lagrange multiplier λ refer to the forces of contact of the LLE with the ground. Hence, the constrained dynamic equation of LLE can be written as (4) [19]:

$$M(q)\ddot{q} + C(q, \dot{q})\dot{q} + G(q) + \tau_d = \tau + J(q)^T \lambda \tag{4}$$

where $J(q) = \frac{\partial \phi(q)}{\partial q}$ stands for the Jacobian of the equation of constraint with:

$$\begin{aligned}
J_1 &= \frac{\partial \phi(q)}{\partial q_1} = -l_1 \sin(q_1) - l_2 \sin(q_1 + q_2) - l_3 \sin(q_1 + q_2 + q_3) \\
J_2 &= \frac{\partial \phi(q)}{\partial q_2} = -l_2 \sin(q_1 + q_2) - l_3 \sin(q_1 + q_2 + q_3), J_3 = \frac{\partial \phi(q)}{\partial q_3} = -l_3 \sin(q_1 + q_2 + q_3)
\end{aligned}$$

This constraint motion makes LLE lose number of degrees of freedoms which are equal to number of constraints [19]. In our work, the LLE is contacting with ground and this thing will make it lose one degree of freedom because of participating of one Algebraic equation. This thing separates the number of the degree of freedom of LLE into two main groups: the first group includes the independent joints coordinates $q_z = [q_1, q_2]^T$, $q_z \in R^2$. whereas the second group includes dependent joint coordinates. $q_N \in R^1$, $q_N = q_3$. Hence, a reduced order model has been obtained that rely on independent joints only (Hip and Knee joints) and the motion of ankle joint will depend on the independents joint motion. If we differentiate the algebraic constraint in (3) with respect to time, we obtain:

$$\dot{\phi}(q) = \frac{d\phi}{dt} = \frac{\partial\phi(q)}{\partial q} \frac{dq}{dt} = J\dot{q} = [J_1\dot{q}_1 + J_2\dot{q}_2 + J_3\dot{q}_3] = 0 \tag{5}$$

the dependent velocity \dot{q}_3 can be expressed in terms of independent velocities \dot{q}_1, \dot{q}_2 as (6).

$$\dot{q}_3 = -J_3(q)^{-1}J_1(q)\dot{q}_1 - J_3(q)^{-1}J_2(q)\dot{q}_2 \tag{6}$$

Hence, velocity coordinates $(\dot{q}_1, \dot{q}_2, \dot{q}_3)$ can be expressed as (7):

$$\begin{bmatrix} \dot{q}_1 \\ \dot{q}_2 \\ \dot{q}_3 \end{bmatrix} = \begin{bmatrix} 1 & 0 \\ 0 & 1 \\ -J_3(q)^{-1}J_1(q) & -J_3(q)^{-1}J_2(q) \end{bmatrix} \begin{bmatrix} \dot{q}_1 \\ \dot{q}_2 \end{bmatrix} \tag{7}$$

thus, we can get (8):

$$\dot{q} = H(q)\dot{q}_z \tag{8}$$

where $\dot{q} = [\dot{q}_1 \quad \dot{q}_2 \quad \dot{q}_3]^T, \dot{q}_z = [\dot{q}_1 \quad \dot{q}_2]^T, H = \begin{bmatrix} 1 & 0 \\ 0 & 1 \\ J_{z1} & J_{z2} \end{bmatrix}, J_{z1} = \frac{J_1(q)}{J_3(q)}, J_{z2} = \frac{J_2(q)}{J_3(q)}$

The generalized acceleration can be written as (9):

$$\ddot{q} = H(q)\ddot{q}_z + \dot{H}(q)\dot{q}_z \tag{9}$$

if we Sub (9) in (4), the dynamic in (4) can be expressed as (10):

$$M(q)H(q)\ddot{q}_z + C_1(q, \dot{q})\dot{q}_z + G(q) + \tau_d = \tau + J(q)^T\lambda \tag{10}$$

where

$$C_1(q, \dot{q}) = C(q, \dot{q})H(q) + M(q)\dot{H}(q) \tag{11}$$

with

$$\dot{H} = \begin{bmatrix} 1 & 0 \\ 0 & 1 \\ J_{z1} & J_{z2} \end{bmatrix}, \dot{J}_{z1} = -\frac{J_3(q)J_1(q) - J_1(q)J_3(q)}{(J_3(q))^2}, \dot{J}_{z2} = -\frac{J_3(q)J_2(q) - J_2(q)J_3(q)}{(J_3(q))^2}$$

and

$$\begin{aligned} J_1(q) &= \psi_1\dot{q}_1 + \psi_2\dot{q}_2 + \psi_3\dot{q}_3, J_2(q) = \psi_2\dot{q}_1 + \psi_2\dot{q}_2 + \psi_3\dot{q}_3, J_3(q) = \psi_3\dot{q}_1 + \psi_3\dot{q}_2 + \psi_3\dot{q}_3 \\ \psi_1 &= -[l_1 \cos(q_1) + l_2 \cos(q_1 + q_2) + l_3 \cos(q_1 + q_2 + q_3)] \\ \psi_2 &= -[l_2 \cos(q_1 + q_2) + l_3 \cos(q_1 + q_2 + q_3)] \\ \psi_3 &= -[l_3 \cos(q_1 + q_2 + q_3)] \end{aligned}$$

According to (10) refers to the reduced order dynamic model for LLE when it contacting with ground. This equation includes $J(q)^T\lambda$ term in its structure. The deleting of this term is very essential for developing an efficient controller. The $J(q)^T\lambda$ term from (10) can be eliminated, by using the expression $J(q)^T H^T(q) = 0$ which is popular property in literature which is used for different fields [22]. If we borrow this property and pre multiply equation (10) by H^T , we can get (12) [23]:

$$\bar{M}(q)\ddot{q}_z + \bar{C}(q, \dot{q})\dot{q}_z + \bar{G}(q) + \bar{\tau}_d = \bar{\tau} \tag{12}$$

With $\bar{M}(q) = H^T M(q)H, \bar{C}(q, \dot{q}) = H^T C_2(q, \dot{q}), \bar{G}(q) = H^T G(q), \bar{\tau} = H^T \tau, \bar{\tau}_d = H^T \tau_d$

3. CONTROLLERS DEVELOPMENTS

In what follows, a sliding mode control scheme (SMC) will be developed in subsection 3.1 which assumes that the tuning of parameters is performed manually by trial and error strategy. Then, in subsection 3.2 a grey wolf optimizer (GWO) will be used in order to get an optimized version of the developed controller (GW-SMC). Later, the description of grey wolf optimizer will be explained in detail in subsection 3.3.

3.1. Sliding mode control (SMC)

Firstly, we present the following sliding manifold:

$$S_z = \dot{e}_z + \Lambda e_z \quad (13)$$

with : $e_z = q_z - q_z^d$, $\dot{e}_z = \dot{q}_z - \dot{q}_z^d$, $S_z = [S_{z1}, S_{z2}]^T$ and $\Lambda \in R^{2 \times 2}$, are positive diagonal matrices. The subscript z stands for independent joint coordinates which are the Hip and Knee joints in our paper. By taking the derivative of (13), one obtains:

$$\dot{S}_z = \ddot{e}_z + \Lambda \dot{e}_z \quad (14)$$

it is essential to enforce the system to be in the sliding surface. Hence, we obtain: $\dot{S}_z = 0$, then we obtain:

$$\ddot{q}_z - \ddot{q}_z^d + \Lambda(\dot{q}_z - \dot{q}_z^d) = 0 \quad (15)$$

by re-writing (12) and dropping dependency, we can get:

$$\ddot{q}_z = \bar{M}^{-1}[\bar{\tau} - \bar{C}\dot{q}_z - \bar{G}] \quad (16)$$

sub (16) in (15), we can obtain:

$$\bar{M}^{-1}[\bar{\tau} - \bar{C}\dot{q}_z - \bar{G}] - \ddot{q}_z^d + \Lambda(\dot{q}_z - \dot{q}_z^d) = 0 \quad (17)$$

if we multiply equation by \bar{M} , we get:

$$[\bar{\tau} - \bar{C}\dot{q}_z - \bar{G}] - \bar{M}\ddot{q}_z^d + \bar{M}\Lambda(\dot{q}_z - \dot{q}_z^d) \quad (18)$$

consequently, we can obtain the following sliding mode control law:

$$\bar{\tau} = \bar{\tau}_{equ} + \bar{\tau}_{sw} \quad (19)$$

with

$$\bar{\tau}_{equ} = \bar{C}\dot{q}_z + \bar{G} + \bar{M}\ddot{q}_z^d - \bar{M}\Lambda(\dot{q}_z - \dot{q}_z^d) \quad (20)$$

$$\bar{\tau}_{sw} = -\bar{M}K_s \text{sgn}(S_z) \quad (21)$$

where: $\bar{\tau}_{sw}$ is a high frequency discontinuous term which has been added to guarantee robustness with $K_s \in R^{2 \times 2}$ is diagonal positive matrix. Thus, we can get the following sliding mode control law.

$$\bar{\tau}_{SMC} = \bar{C}\dot{q}_z + \bar{G} + \bar{M}\ddot{q}_z^d - \bar{M}\Lambda(\dot{q}_z - \dot{q}_z^d) - \bar{M}K_s \text{sgn}(S_z) \quad (22)$$

If we sub (22) in (14) we get:

$$\dot{S}_z = \bar{\tau}_{sw} \bar{M}^{-1} \quad (23)$$

the lyapunov function related to dynamic system of LLE is:

$$V = \frac{1}{2} S_z^T S_z \quad (24)$$

the main aim of this selection is ensure the minimization process of $S_z = 0$. In addition, to remain on sliding surface and to ensure that the the error e_z will convergence to zero. Hence, if we differntate V with respect to time, we get:

$$\dot{V} = S_z^T \dot{S}_z \quad (25)$$

$$\dot{V} = S_z^T \bar{\tau}_{sw} \bar{M}^{-1} \quad (26)$$

$$\dot{V} = -S_z^T K_s \text{sgn}(S_z) < 0 \tag{27}$$

One of the main drawbacks of the sliding mode control is the existing of chattering problem which may cause the damage of the actuators. For eliminating and overcoming the influence of chattering effects, we replace the sign function by a smooth hyperbolic tangent function which has [24].

$$\tanh(S_z) = \frac{e^{S_z} - e^{-S_z}}{e^{S_z} + e^{-S_z}} \tag{28}$$

3.2. Optimal sliding mode control (GW-SMC)

As shown in (22), the tuning of controller parameters of SMC (Λ, K_s) has been usually performed using trial and error method. In fact, this is an exhausted process. For solving this tedious method, a meta-heuristic optimization technique called grey wolf optimizer (GWO) presented in detail in sub-section 3.3 is used to tune the gains of SMC controller. Hence, we get a GW-SMC controller which can be expressed as:

$$\bar{\tau}_{GW-SMC} = \bar{C} \dot{q}_z + \bar{G} + \bar{M} \ddot{q}_z^d - \bar{M} \Lambda^* (\dot{q}_z - \dot{q}_z^d) - \bar{M} K_s^* \text{sgn}(S_z) \tag{29}$$

where: (Λ^*, K_s^*), represent optimized values of SMC parameters. The block diagram of SMC optimized by grey wolf optimizer (GWO) is shown in Figure 2.

3.3. Grey wolf optimizer algorithm (GWO)

A grey wolf optimizer algorithm (GWO) is a relatively new swarm population-based optimization algorithm developed in 2014 by Faris *et al.* [25]. The work of GWO mainly depends on simulating the social behavior of grey wolves that lived in the wild by considering the concept of the leadership hierarchy and the mechanism hunting to the prey of grey wolf. In this algorithm, a grey wolf hierarchy has been classified into four types of wolves: Alpha (α) wolf, Beta (β) wolf, Delta (δ) wolf and Omega (ω) wolf. The hunting process decision is achieved by leaders of whole group which is Alpha (α) wolf. Beta (β) wolf follows the commands of Alpha (α) wolf and help it in decision of hunting and other activities in the pack. Omega (ω) wolf will lead the other Omegas (ω) and will follow Alphas (α), and Betas (β) wolves. If the wolf it is not an Alpha (α), Beta (β), or Omega (ω), the wolf will be named as Delta (δ) wolf. The optimal solution which is representing the location of prey will be implemented by estimating the populations of wolves by using an iterative method. The best wolf is an Alpha (α) wolf, the best second solution stands for Beta (β) and Delta (δ) is third-best solution whereas Omega (ω) wolves are the least significant solutions. Equations (30) and (31) have been used for formulating a mathematical model that describes the behavior of wolves in encircling process (finding the optimum solutions):

$$\vec{D} = |\vec{C} \vec{X}_p(t) - \vec{X}(t)| \tag{30}$$

$$\vec{X}(t + 1) = |\vec{X}_p(t) - \vec{A} \vec{D}| \tag{31}$$

where t refer to current iteration, \vec{A} and \vec{C} are coefficient vectors, $\vec{X}_p(t)$ stands for the prey victim position vectors. Whereas $\vec{X}(t)$ is the position vector of a grey wolf. The calculation of vectors \vec{A} and \vec{C} can be expressed as:

$$\vec{A} = 2\vec{a} \vec{r}_1 - \vec{a} \tag{32}$$

$$\vec{C} = 2\vec{r}_2 \tag{33}$$

\vec{r}_1, \vec{r}_2 stands for vectors in random with range between 0 and 1, \vec{a} decreased from 2 to 0 in linear manner during the iterations process. The updating process can be expressed as:

$$\vec{D}_\alpha = |\vec{C}_1 \vec{X}_\alpha(t) - \vec{X}|, \vec{D}_\beta = |\vec{C}_2 \vec{X}_\beta(t) - \vec{X}|, \vec{D}_\delta = |\vec{C}_3 \vec{X}_\delta(t) - \vec{X}| \tag{34}$$

$$\vec{X}_1 = |\vec{X}_\alpha - \vec{A}_1 \vec{D}_\alpha|, \vec{X}_2 = |\vec{X}_\beta - \vec{A}_2 \vec{D}_\beta|, \vec{X}_3 = |\vec{X}_\delta - \vec{A}_3 \vec{D}_\delta| \tag{35}$$

$$\vec{X}(t + 1) = \frac{\vec{X}_1 + \vec{X}_2 + \vec{X}_3}{3} \tag{36}$$

the details of Pseudo code of GWO can be found in [25]. An integral time absolute error (ITAE) expressed in (37) has been used as an objective function to evaluate the position of each search agents (wolves) during the search for choosing the best value [17].

$$ITAE = \int_0^T t|e| dt \tag{37}$$

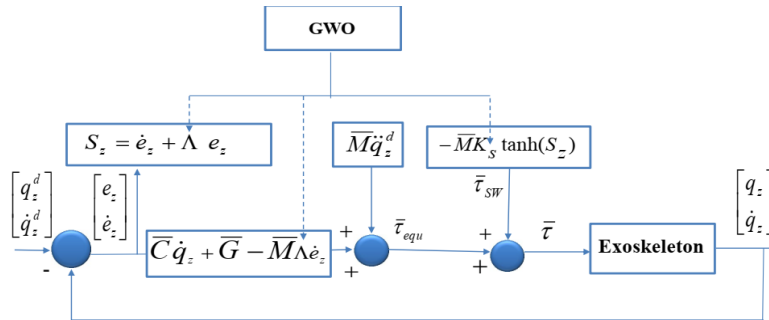


Figure 2. Block diagram of sliding mode controller optimized by GWO (GW-SMC)

4. RESULTS AND DISSCUSION

This section is dedicated for comparing the effectiveness of developed optimal sliding mode controller GW-SMC derived in the previous section with recently developed SMC with chateering suppressor which is developed in [26]. The desired trajectories are taken from [27]. The parameters of human and exoskeleton that used in simulation are adopted from [28] and listed in Table 1. Moreover, the integral absolute value error (IAE) and integrated squared error ISE have been used as a measure for tracking performances of SMC and GW-SMC controllers.

$$IAE = \int |e| dt \tag{38}$$

$$ISE = \int e^T e dt \tag{39}$$

The parameters values SMC controller with with chateering suppressor has been selected by trial and error method. For GW-SMC controllers, the parameters selected as $\Lambda = 25.73, K_s = 8.22$ and have been tuned using GWO. The number of wolves chosen is 50 and the algorithms are repeated for 70 iterations. Figure 3 explain the excellent Objective Function performance of GWO after 70 iterations. The cmpparative simulation results are explained for three cases: nominal, uncertainty and disturbance rejection tests.

Table 1. Physical parameters of human and lower limb exoskeleton [28]

parameter	Mass (m) in kg		Length (l) in m		Inertia (I)in kg.m ²		Center of length (d) m	
	Exoskeleton	Human	Exoskeleton	Human	Exoskeleton	Human	Exoskeleton	Human
Thigh	0.2043	7.33	0.41	0.407	5.7×10-3	0.1502	0.15	0.1763
Shank	0.2159	3.4503	0.39	0.4334	4.3×10-3	0.0505	0.11	0.1849
Foot	0.115	1.075	0.159	0.275	3.9×10-4	0.0038	0.04	0.1179

4.1. Nominal case

The evolutions of position, position error, and torque input signal for hip and knee joints for SMC in [26] and GW-SMC controllers in nominal case are depicted in Figures 4 and 5 respectivaly. It is worth to observe the validity of the GW-SMC controller over SMC controller with chateering suppressor in [26] in terms of trajectory tracking performance and minimization the tracking errors. This refelects the vital role of GWO in finding the optimal values and its impact to the system performance. A smooth control input signals have been obtained for two controllers owing to existing hyperbolic function which has the ability to reduce the chattering effect effectively. The results of IAE index and ISE performance indices for nominal cases for SMC in [26] and GW-SMC controllers are shown in Table 2. The results explain that GW-SMC controller has lowest tracking error as compared with SMC controller with chateering suppressor.

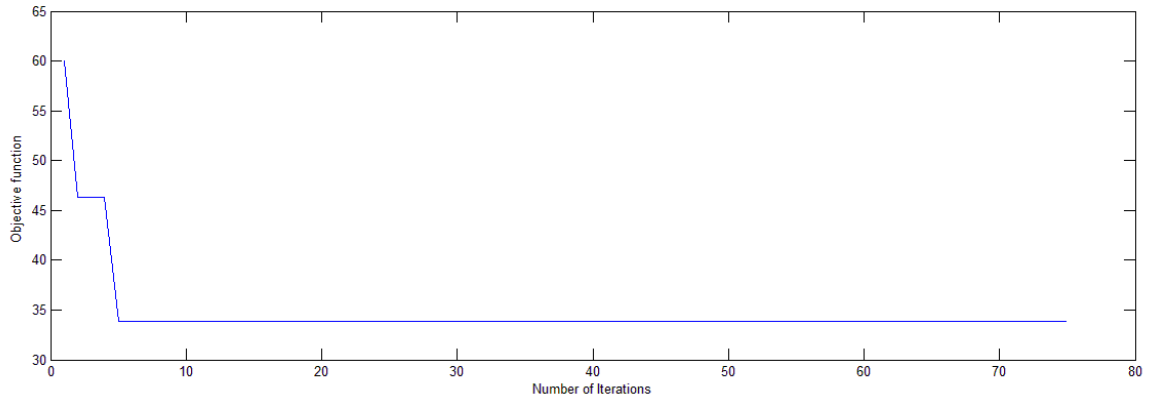


Figure 3. Evolution of objective function of grey wolf optimizer after 70 iterations

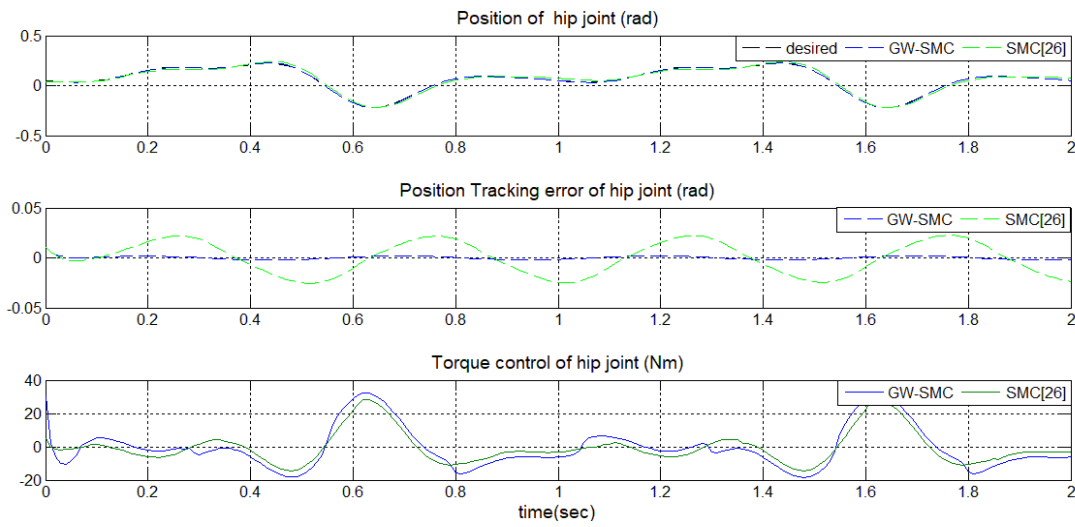


Figure 4. Performance of hip joint for two controllers in nominal case

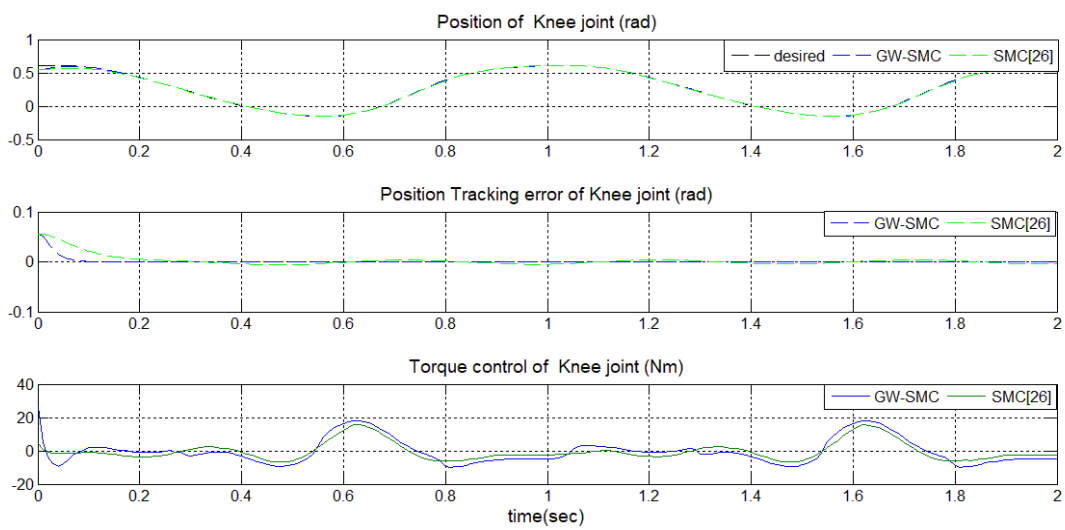


Figure 5. Performance of Knee joint for two controllers in nominal case

Table 2. Performance indices IAE and ISE for two controllers for nominal case

Index	IAE		ISE	
	GW-SMC (29)	SMC [26]	GW-SMC (29)	SMC [26]
Hip joint	0.001372	0.013715	0.001654	0.01571
Knee joint	0.001541	0.005277	0.006407	0.01068
Both joints	0.002914	0.018992	0.008062	0.02640

4.2. Uncertainty case

In this case, the parameters of the LLE are varied by 30% from their original nominal values. It is observed from Figures 6 and 7 and Table 3 that GW-SMC controller has an excellent robustness against system uncertainty. The figures and table illustrate that the performance of SMC with with chattering suppressor is significantly changed in case of the presence of parameters variations while the proposed GW-SMC is remain insensitive to parameter variations.

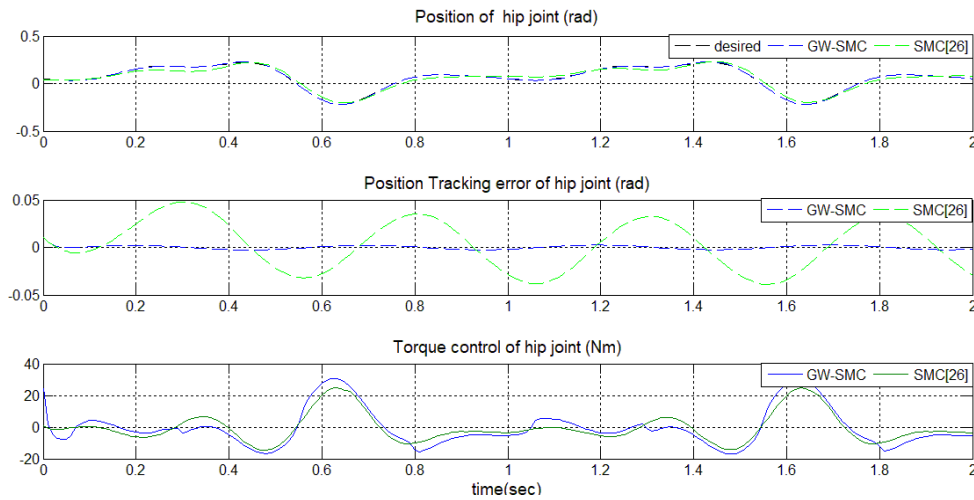


Figure 6. Performance of hip joint for two controllers in uncertainty case

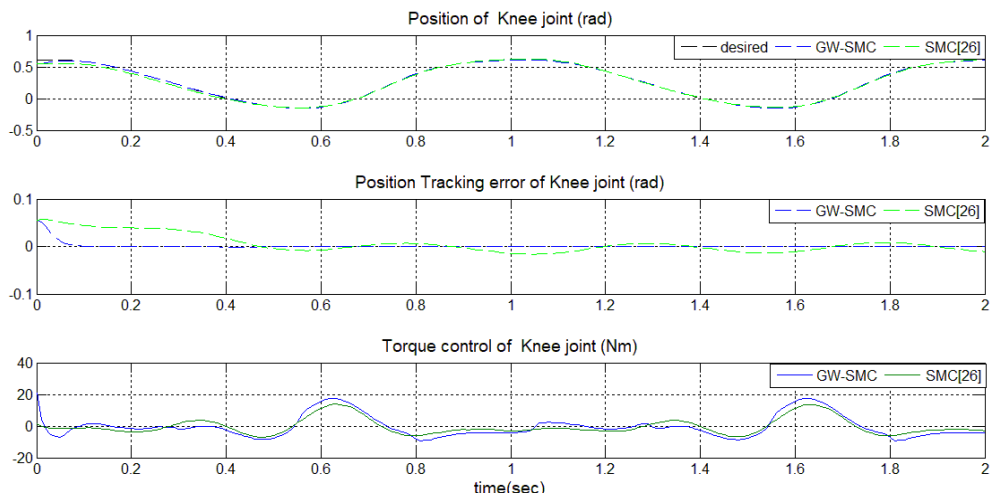


Figure 7. Performance of Knee joint for two controllers in uncertainty case

Table 3. Performance indices IAE and ISE for two controllers for uncertainty case

Index	IAE		ISE	
	GW-SMC (29)	SMC [26]	GW-SMC (29)	SMC [26]
Hip joint	0.001649	0.021897	0.001933	0.02523
Knee joint	0.001705	0.013445	0.006690	0.01962
Both joints	0.003355	0.035342	0.008623	0.04486

4.3. Disturbance rejection case

The third simulation has been achieved in the presence of time varying disturbance which has the following expression [29].

$$\tau_d = \begin{bmatrix} \tau_{d1} \\ \tau_{d2} \end{bmatrix} = \begin{bmatrix} 2 \sin(t) + 0.5 \sin(100t) \\ \cos(t) + 0.5 \sin(100t) \end{bmatrix} \tag{40}$$

We can notice from Figures 8 and 9 that smaller control errors and faster convergence have been effectively ensured by GW-SMC as compared with the SMC with chattering suppressor in [26]. Thanks to tuning process by GWO our GW-SMC controller can still ensure the best comprehensive control performance and it is still satisfactory in spite of the presence external disturbances. The tracking control performance indices IAE and ISE for this case are given in Table 4. We can notice that the GW-SMC has the lower best values in terms of IAE and ISE performance indices as compared with SMC with chattering suppressor. To sum up, the advantages and the superiority performance of the proposed GW-SMC controller have been verified. GW-SMC controller provides an excellent tracking performance; high precise tracking, less chattering and good robustness towards the uncertainties and external disturbances.

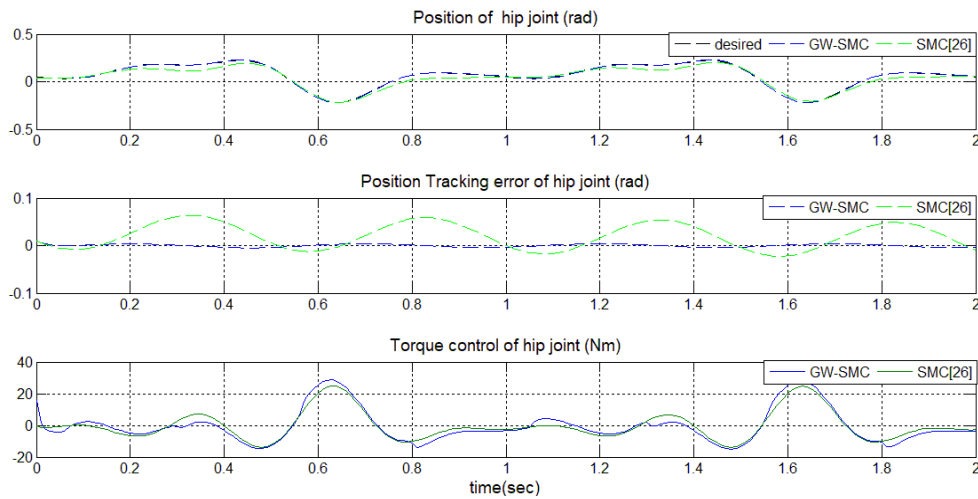


Figure 8. Performance of hip joint for two controllers in disturbance rejection case

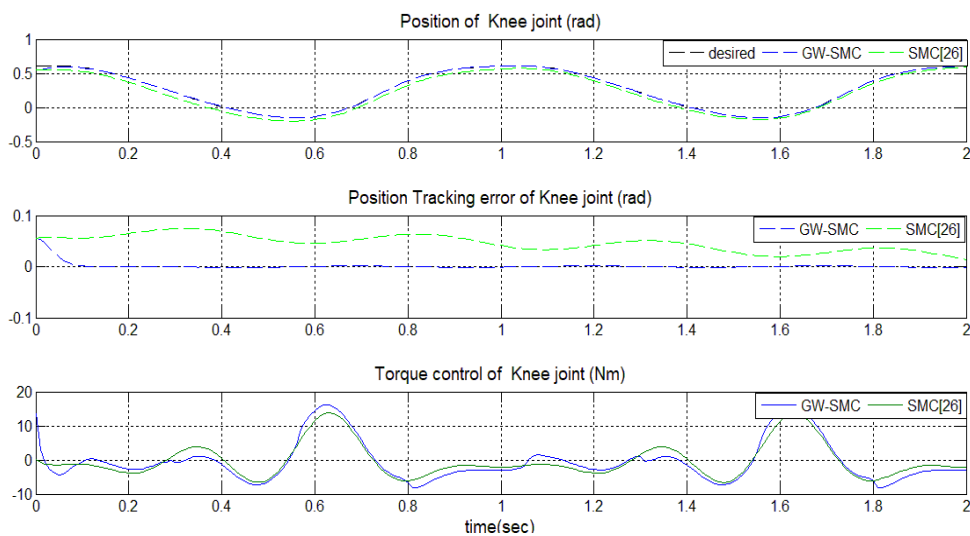


Figure 9. Performance of Knee joint for two controllers in disturbance rejection case

Table 4. Performance indices IAE and ISE for two controllers for disturbance rejection case

Index Controller	IAE		ISE	
	GW-SMC (29)	SMC [26]	GW-SMC (29)	SMC [26]
Hip joint	0.0026758	0.026384	0.003066	0.032597
Knee joint	0.002160	0.046239	0.007396	0.048754
Both joints	0.004836	0.072624	0.010463	0.081352

5. CONCLUSION

In this study, a reduced order constraint model with augmented Lagrange equations for a lower limb exoskeleton in constrained circumstances dedicated for rehabilitation of stroke patients have been developed. Optimal sliding mode controller tuned by grey wolf optimization algorithm (GW-SMC) has been developed to control lower limb exoskeleton in constrained environments. The stability analysis of the closed-loop system has been performed using Lyapunov theory of stability. Simulation results in nominal, uncertain and disturbance rejection tests indicate that the sliding mode controller optimized by grey wolf optimizer provides excellent results performances in terms of robustness, fast response and tracking error as compared with conventional sliding mode controller. In the Future, the focusing will be on extending this controller in real time rehabilitation exoskeleton systems and using another types of optimization algorithm for tuning the controller parameters. We are planning to combine this controller with fractional order calculus for getting an excellent response of the performance of the system.




REFERENCES

- [1] S. K. Hasan and A. K. Dhingra, "State of the art technologies for exoskeleton human lower extremity rehabilitation robots," *Journal of Mechatronics and Robotics*, vol. 4, no. 1, pp. 211–235, Jan. 2020, doi: 10.3844/jmrsp.2020.211.235.
- [2] W. Meng, Q. Liu, Z. Zhou, Q. Ai, B. Sheng, and S. S. Xie, "Recent development of mechanisms and control strategies for robot-assisted lower limb rehabilitation," *Mechatronics*, vol. 31, pp. 132–145, Oct. 2015, doi: 10.1016/j.mechatronics.2015.04.005.
- [3] X. Zhang, Z. Yue, and J. Wang, "Robotics in lower-limb rehabilitation after stroke," *Behavioural Neurology*, vol. 2017, pp. 1–13, 2017, doi: 10.1155/2017/3731802.
- [4] M. Bernhardt, M. Frey, G. Colombo, and R. Riener, "Hybrid force-position control yields cooperative behaviour of the rehabilitation robot LOKOMAT," in *Proceedings of the 2005 IEEE 9th International Conference on Rehabilitation Robotics*, 2005, vol. 2005, pp. 536–539, doi: 10.1109/ICORR.2005.1501159.
- [5] S. K. Banala, S. H. Kim, S. K. Agrawal, and J. P. Scholz, "Robot assisted gait training with active leg exoskeleton (ALEX)," *IEEE Transactions on Neural Systems and Rehabilitation Engineering*, vol. 17, no. 1, pp. 2–8, Feb. 2009, doi: 10.1109/TNSRE.2008.2008280.
- [6] H. Kazerooni, R. Steger, and L. Huang, "Hybrid control of the Berkeley lower extremity exoskeleton (BLEEX)," *International Journal of Robotics Research*, vol. 25, no. 5–6, pp. 561–573, 2006, doi: 10.1177/0278364906065505.
- [7] N. A. Alawad, A. J. Humaidi, and A. S. Alaraji, "Fractional proportional derivative-based active disturbance rejection control of knee exoskeleton device for rehabilitation care," *Indonesian Journal of Electrical Engineering and Computer Science*, vol. 28, no. 3, pp. 1405–1413, 2022, doi: 10.11591/ijeecs.v28.i3.pp1405-1413.
- [8] M. A. Faraj and A. M. Abbood, "Fractional order PID controller tuned by bat algorithm for robot trajectory control," *Indonesian Journal of Electrical Engineering and Computer Science*, vol. 21, no. 1, pp. 74–83, Jan. 2021, doi: 10.11591/ijeecs.v21.i1.pp74-83.
- [9] M. A. Faraj, B. Maalej, N. Derbel, and M. Deriche, "Modeling and robust computed torque control for lower limb exoskeleton contacting with ground," in *2022 19th IEEE International Multi-Conference on Systems, Signals and Devices, SSD 2022*, May 2022, pp. 571–579, doi: 10.1109/SSD54932.2022.9955781.
- [10] Y. Zhang, G. Cao, W. Li, J. Chen, L. Li, and D. Diao, "A self-adaptive-coefficient-double-power sliding mode control method for lower limb rehabilitation exoskeleton robot," *Applied Sciences (Switzerland)*, vol. 11, no. 21, p. 10329, Nov. 2021, doi: 10.3390/app112110329.
- [11] S. Ahmed, H. Wang, and Y. Tian, "Model-free control using time delay estimation and fractional-order nonsingular fast terminal sliding mode for uncertain lower-limb exoskeleton," *JVC/Journal of Vibration and Control*, vol. 24, no. 22, pp. 5273–5290, Nov. 2018, doi: 10.1177/1077546317750978.
- [12] S. Han, H. Wang, and Y. Tian, "Model-free based adaptive nonsingular fast terminal sliding mode control with time-delay estimation for a 12 DOF multi-functional lower limb exoskeleton," *Advances in Engineering Software*, vol. 119, pp. 38–47, May 2018, doi: 10.1016/j.advengsoft.2018.01.004.
- [13] M. Mokhtari, M. Taghizadeh, and M. Mazare, "Impedance control based on optimal adaptive high order super twisting sliding mode for a 7-DOF lower limb exoskeleton," *Meccanica*, vol. 56, no. 3, pp. 535–548, Mar. 2021, doi: 10.1007/s11012-021-01308-4.
- [14] M. Mokhtari, M. Taghizadeh, and M. Mazare, "Hybrid adaptive robust control based on CPG and ZMP for a lower limb exoskeleton," *Robotica*, vol. 39, no. 2, pp. 181–199, Feb. 2021, doi: 10.1017/S0263574720000260.
- [15] M. Mazare, M. Taghizadeh, and P. Ghaf-Ghanbari, "Fault-tolerant control based on adaptive super-twisting nonsingular integral-type terminal sliding mode for a delta parallel robot," *Journal of the Brazilian Society of Mechanical Sciences and Engineering*, vol. 42, no. 8, p. 443, Aug. 2020, doi: 10.1007/s40430-020-02510-3.
- [16] M. Mazare, M. Taghizadeh, and P. Ghaf-Ghanbari, "Pitch actuator fault-tolerant control of wind turbines based on time delay control and disturbance observer," *Ocean Engineering*, vol. 238, p. 109724, Oct. 2021, doi: 10.1016/j.oceaneng.2021.109724.
- [17] A. Rezoug, J. Iqbal, and M. Tadjine, "Extended grey wolf optimization-based adaptive fast nonsingular terminal sliding mode control of a robotic manipulator," *Proceedings of the Institution of Mechanical Engineers. Part I: Journal of Systems and Control Engineering*, vol. 236, no. 9, pp. 1738–1754, Oct. 2022, doi: 10.1177/09596518221099768.
- [18] M. W. Spong, S. Hutchinson, and M. Vidyasagar, *Robot Modeling and Control [Book Review]*, vol. 26, no. 6. John Wiley & Sons, 2006, doi: 10.1109/MCS.2006.252815.




- [19] R. M. Murray, Z. Li, and S. Shankar Sastry, *A mathematical introduction to robotic manipulation*, vol. 26, no. 6. CRC Press, 2017, doi: 10.1201/9781315136370.
- [20] A. Chemori and A. Loria, "Control of a planar underactuated biped on a complete walking cycle," *IEEE Transactions on Automatic Control*, vol. 49, no. 5, pp. 838–843, May 2004, doi: 10.1109/TAC.2004.828314.
- [21] J. Zhang, Y. Dong, C. Yang, Y. Geng, Y. Chen, and Y. Yang, "5-Link model based gait trajectory adaption control strategies of the gait rehabilitation exoskeleton for post-stroke patients," *Mechatronics*, vol. 20, no. 3, pp. 368–376, Apr. 2010, doi: 10.1016/j.mechatronics.2010.02.003.
- [22] A. Burghardt and W. Skwarek, "Modeling the dynamics of two cooperating robots," *Applied Sciences*, vol. 11, no. 13, p. 6019, Jun. 2021, doi: 10.3390/app11136019.
- [23] N. Kumar and M. Rani, "Neural network-based hybrid force/position control of constrained reconfigurable manipulators," *Neurocomputing*, vol. 420, pp. 1–14, Jan. 2021, doi: 10.1016/j.neucom.2020.09.009.
- [24] B. Maalej, A. Chemori, and N. Derbel, "Towards an effective robotic device for gait rehabilitation of children with cerebral palsy," in *2019 International Conference on Signal, Control and Communication (SCC)*, Dec. 2019, pp. 268–273, doi: 10.1109/SCC47175.2019.9116141.
- [25] H. Faris, I. Aljarah, M. A. Al-Betar, and S. Mirjalili, "Grey wolf optimizer: a review of recent variants and applications," *Neural Computing and Applications*, vol. 30, no. 2, pp. 413–435, Jul. 2018, doi: 10.1007/s00521-017-3272-5.
- [26] S. K. Hasan and A. K. Dhingra, "Development of a sliding mode controller with chattering suppressor for human lower extremity exoskeleton robot," *Results in Control and Optimization*, vol. 7, p. 100123, Jun. 2022, doi: 10.1016/j.rico.2022.100123.
- [27] S. Mefoued, "Commande robuste référencée intention d'une orthèse active pour l'assistance fonctionnelle aux mouvements du genou," Ph.D. dissertation, Université Paris-Est, 2012.
- [28] M. S. Amiri, R. Ramli, M. F. Ibrahim, D. A. Wahab, and N. Aliman, "Adaptive particle swarm optimization of PID gain tuning for lower-limb human exoskeleton in virtual environment," *Mathematics*, vol. 8, no. 11, p. 2040, Nov. 2020, doi: 10.3390/math8112040.
- [29] S. Ahmed, H. Wang, and Y. Tian, "Robust adaptive fractional-order terminal sliding mode control for lower-limb exoskeleton," *Asian Journal of Control*, vol. 21, no. 1, pp. 473–482, Jan. 2019, doi: 10.1002/asjc.1964.

BIOGRAPHIES OF AUTHORS






Mohammad A. Faraj    born in AL-Anbar, Iraq in 1982. In 2004, he received the B.Sc. degree from university of technology, control and systems engineering department, Baghdad, Iraq. He received the M.Sc. degree in mechatronics engineering specialization from University of Technology, control and systems engineering department in 2008. He works as a Lecturer at department of electrical engineering, university of Al-Anbar, Iraq since 2008. Currently; he is a Ph.D. student at University of Sfax, National Engineering School of Sfax (ENIS), Tunisia. His research interests include: adaptive and robust control, nonlinear control, robotic manipulator, Rehabilitation exoskeleton robots and optimization algorithms. He can be contacted at email: mohammed.faraj@uoanbar.edu.iq.



Boutheina Maalej    was born in Tunisia in 1992. She received the Engineering Diploma and the Doctorate degrees in Electrical Engineering from the University of Gabes, Tunisia, in 2016 and 2021, respectively. She is a member of Control and Energy Management laboratory of ENIS in Sfax. She is involved in postgraduate research development in control robotic systems at ENIS. She also served as committee member of several IEEE conferences. She is also an IEEE member. Her research interests are in the areas of nonlinear control systems. She can be contacted at email: maalej.boutheina@gmail.com.



Nabil Derbel    was born in Sfax (Tunisia) in April 1962. He received his engineering Diploma from the Ecole Nationale d'Ingénieurs de Sfax in 1986, the Diplôme d'Études Approfondies in Automatic control from the Institut National des Sciences Appliquées de Toulouse in 1986, the Doctorat d'Université degree from the Laboratoire d'Automatique et d'Analyse des Systèmes de Toulouse in 1989, and the Doctorat d'Etat degree from the Ecole Nationale d'Ingénieurs de Tunis. He joined the Tunisian University in 1989, where he held different positions involved in research and education. Currently, he is a full Professor (First Class) of Automatic Control at the Ecole Nationale d'Ingénieurs de Sfax. His current interests include: optimal control, complex systems, robotic systems, and power systems. He can be contacted at email: nabil.derbel@enis.tn.